Proc. Natl. Acad. Sci. USA
Vol. 91, pp. 4034–4038, April 1994
Biochemistry

The structure of bacteriophage T7 lysozyme, a zinc amidase and an inhibitor of T7 RNA polymerase

XIAODONG CHENG*, XING ZHANG†, JAMES W. PFLUGRATH*, AND F. WILLIAM STUDIER†

*W. M. Keck Structural Biology Laboratory, Cold Spring Harbor Laboratory, Cold Spring Harbor, NY 11724; and †Biology Department, Brookhaven National Laboratory, Upton, NY 11973

Contributed by F. William Studier, December 28, 1993

ABSTRACT **The lysozyme of bacteriophage T7 is a bifunctional protein that cuts amide bonds in the bacterial cell wall and binds to and inhibits transcription by T7 RNA polymerase. The structure of a mutant T7 lysozyme has been determined by x-ray crystallography and refined at 2.2-Å resolution. The protein folds into an α/β-sheet structure that has a prominent cleft. A zinc atom is located in the cleft, bound directly to three amino acids and, through a water molecule, to a fourth. Zinc is required for amidase activity but not for inhibition of T7 RNA polymerase. Alignment of the zinc ligands of T7 lysozyme with those of carboxypeptidase A and thermolysin suggests structural similarity among the catalytic sites for the amidase and these zinc proteases. Mutational analysis identified presumed catalytic residues for amidase activity within the cleft and a surface that appears to be the site of binding to T7 RNA polymerase. Binding of T7 RNA polymerase inhibits amidase activity.**

Although named for its lytic activity, T7 lysozyme also binds specifically to T7 RNA polymerase and inhibits transcription (1). This interaction provides a feedback mechanism that shuts off late transcription during T7 infection and also stimulates DNA replication (refs. 1–4; X.Z. and F.W.S., unpublished data). The ability to inhibit transcription has made T7 lysozyme widely used for controlling basal expression in a gene expression system based on T7 RNA polymerase (5, 6). T7 lysozyme differs from the previously well-studied egg-white and phage T4 lysozymes not only in having an interaction with T7 RNA polymerase but also in the chemistry of lysis: it cuts the amide bond between *N*-acetylmuramic acid and L-alanine rather than the glycosidic bond between *N*-acetylmuramic acid and *N*-acetylglucosamine in the peptidoglycan layer of bacterial cell walls (7). We expected that knowledge of the structure of T7 lysozyme would help us to understand how its dual activities are accommodated in a protein of only 150 amino acids (8).

EXPERIMENTAL PROCEDURES

Expression, Purification, and Crystallization. Base pairs 10,706–11,161 of T7 DNA code for T7 lysozyme (8). Sequencing of lysozyme clones revealed that nucleotides 11,061 and 11,062 of T7 DNA are TG instead of GT, a result confirmed in wild-type T7 DNA. Therefore, amino acid 118 of T7 lysozyme is predicted to be valine instead of glycine, as also observed in the crystal structure. An *Ava* II–*Ase* I fragment (base pairs 10,664–11,164) was cloned between the $\phi 10$ promoter and Tϕ terminator for T7 RNA polymerase in the pET-3 expression vector (6) to give plasmid pAR4593, the source of wild-type lysozyme. The AK6 mutation, which deletes amino acids 2–5 of wild-type lysozyme, was made by joining a *Dra* I–*Eco*RI fragment coding for amino acids 6–150 of T7 lysozyme (from pAR4593) to the *Nhe* I–*Eco*RI fragment that contains the T7*lac* promoter and s*10* translation start from pET-11d (6), producing pAR4617. The *Nhe* I site of the latter fragment was partly filled in, using G and A, and the protruding A and G were trimmed with mung bean nuclease before blunt-end ligation, so that the initiating Met-Ala was fused to Lys^6 of T7 lysozyme. Wild-type or AK6 mutant lysozyme was produced from these plasmids in *Escherichia coli* HMS174(DE3) by inducing T7 RNA polymerase with isopropyl β-D-thiogalactopyranoside as described (6).

Purification of the proteins was modified from that previously described for T7 lysozyme (1). Cleared lysate was passed through a DE52 column (Whatman), and the flow-through was applied to a Mono S column (Pharmacia FPLC) and eluted with a gradient of 10–400 mM NaCl. Buffers contained 0.1 mM $ZnSO_4$. Crystals of AK6 lysozyme were grown by mixing 5 μl of protein solution (10 mg/ml in 20 mM Hepes, pH 7.0/250 mM NaCl/0.1 mM $ZnSO_4$/5 mM 2-mercaptoethanol) with an equal volume of 20% (wt/vol) polyethylene glycol 4000/50 mM ammonium sulfate/50 mM sodium citrate at pH 6.6 and equilibrating the mixture against 1 ml of the latter solution.

Mercuric chloride derivatives were obtained by growing crystals in mother liquor saturated with mercuric chloride, since the conventional soaking method caused cracking of already formed crystals. The cocrystals were isomorphous and showed a single mercury site in both difference and anomalous Patterson maps. Derivatives were also obtained by soaking native crystals in 0.5 mM *p*-chloromercuribenzenesulfonic acid for 1 week. Both mercury compounds reacted with Cys^{18}.

Data Collection and Structure Determination. Crystallographic information for AK6 mutant lysozyme is given in Table 1.‡ The diffraction intensities were measured at 16°C on a FAST area detector with CuK_α radiation (1.54 Å) generated by an Elliott GX-21 rotating anode: the exposure times were 100–180 sec for 0.1° of rotation at 45 kV and 95 mA, and the detector was run at a gain setting of SETDET 7 7. Data acquisition and processing were under the control of MADNES software (9). Each reflection profile was analyzed by the method of Kabsch (10). The data sets were divided into sectors each containing roughly 1000–2000 reflections for scaling with the program FS (11). Heavy-atom parameters were refined and initial phases were calculated with the program PROTEIN (12). The model was built by using the program FRODO (13) with three rounds of phase combination of the atomic model with the MIRAS phase using COMBINE (written by W. Kabsch). The initial atomic model was refined against 2.5-Å native data by using the program X-PLOR (14). One hundred steps of Powell optimization smoothly reduced the *R* factor from 0.40 to 0.277 with no manual intervention. One cycle of simulated annealing refinement was then carried

The publication costs of this article were defrayed in part by page charge payment. This article must therefore be hereby marked "*advertisement*" in accordance with 18 U.S.C. §1734 solely to indicate this fact.

‡The atomic coordinates have been deposited in the Protein Data Bank, Chemistry Department, Brookhaven National Laboratory, Upton, NY 11973 (reference 1LBA).

Table 1. X-ray data from crystals of AK6 mutant T7 lysozyme ($F > 2\sigma_F$)

	Native	$HgCl_2$	p-Chloromercuribenzenesulfonate
Resolution, Å	2.2	2.5	2.8
No. of reflections			
Observed	42,968	24,579	7,270
Unique	7,142	3,582	3,055
R_{merge},* %	8.61	9.30	5.07
No. of crystals	5	5	2
Phasing power (2.5 Å)†	—	3.77	2.73
Mean figure of merit	0.80		

*$R_{merge} = \Sigma|I - \langle I\rangle|/\Sigma\langle I\rangle$, where I is the observed intensity and $\langle I\rangle$ is the averaged intensity obtained from multiple observations of symmetry-related reflections.

†Phasing power = rms $(\langle F_H\rangle/E)$, where F_H is the heavy-atom structure-factor amplitude and E is residual lack of closure.

out, using initial and final temperatures of 3000 K and 350 K, respectively, reducing the R factor to 0.24. A total of five rounds of manual rebuilding using FRODO and least-squares refinement using X-PLOR were then carried out. The resolution of the native data was extended to 2.2 Å, and only 26 well-resolved bound water molecules were included. The R factor is 0.19 for 6991 reflections within the resolution range of 10 to 2.2 Å. The final model has root-mean-square deviations from ideal bond distances and angles of 0.017 Å and 3.3°, respectively. All main-chain ϕ and ψ angles are within allowed regions.

The data sets of wild-type T7 lysozyme were collected using 1.15-Å wavelength at beamline X12-C at the National Synchrotron Light Source, Brookhaven National Laboratory. The refined AK6 coordinates were used as the initial model of the wild-type lysozyme and refined for 4067 unique reflections measured between 10 to 2.7 Å with $F > 2\sigma_F$. Positional refinement, with the program X-PLOR, reduced the R factor from 0.427 to 0.276.

Assay of Amidase Activity. Amidase activity was assayed by measuring the decrease in turbidity of *E. coli* C600 cells that had been incubated in 0.1 M EDTA for 5 min at room temperature, pelleted, suspended in 10 mM potassium phosphate (pH 7.0), and kept on ice until use (15). A few minutes before assay, lysozyme fractions (about 1 mg/ml) were diluted on ice in 20 mM Hepes, pH 7.0/10 mM NaCl/5 mM 2-mercaptoethanol containing bovine serum albumin (100 μg/ml) and either 2 mM EDTA or 2 mM $ZnSO_4$. To measure activity, 10 μl of diluted enzyme was added to 1 ml of sensitized cells that had been brought to room temperature, and the change in OD_{600} was recorded at intervals. Enzyme dilutions that decreased the turbidity at a maximum rate of about 0.02–0.04 OD_{600} unit/min were used to calculate activities; 1 unit of activity was defined as the amount of enzyme that reduced OD_{600} at the rate of 0.001/min.

RESULTS AND DISCUSSION

Crystallization and Structure Determination. Attempts to crystallize wild-type T7 lysozyme were initially unsuccessful, but a mutant lysozyme that lacks four amino acids near the N terminus crystallized readily. This mutant, AK6, lacks amino acids 2–5 (Arg-Val-Gln-Phe) of the wild-type protein. The mutant protein has normal amidase activity but is completely unable to bind or inhibit T7 RNA polymerase.

The AK6 mutant protein was produced from the cloned gene and purified in the presence of Zn^{2+} because T7 lysozyme had been found to contain zinc (J. Flanagan and K. MacKenzie, personal communication). Under appropriate conditions, crystals of the purified protein began to appear within 10 min and reached a size of 0.5 mm × 0.6 mm × 1.5 mm overnight. The crystals formed in space group $C222_1$ with unit cell dimensions a = 46.5 Å, b = 62.5 Å, and c = 110.0 Å. There is one molecule in each of the eight asymmetric units. Initial 2.5-Å phases were obtained by multiple isomorphous replacement from two mercury derivatives together with their anomalous scattering contributions (Table 1). The phases produced electron density maps that enabled us to trace the polypeptide backbone and fit the complete sequence of 146 amino acids.

We also obtained crystals of wild-type T7 lysozyme by seeding first with microcrystals of AK6 mutant protein and then with microcrystals of the wild-type protein. These crystals took weeks rather than hours to grow and diffracted to a resolution of about 2.7 Å. They were isomorphous to the AK6 crystals, and the wild-type structure was solved by difference Fourier analysis. The only significant difference was at the N terminus, where the wild-type protein has four additional residues. The N-terminal residues of the AK6 structure are flexible (higher temperature factor), and the additional residues in the wild-type structure are completely disordered.

Protein Structure. Two views of the structure of the AK6 mutant lysozyme and a diagram of the locations of structural elements in the amino acid sequence are shown in Fig. 1. The protein contains five β-strands and three α-helices, designated β1, αA, β2, β3, β4, αB, β5, and αC in order from N to C terminus of the amino acid sequence. The loops between these structures are designated 1A, A2, 23, 34, 4B, B5, and 5C. The structure contains a central sheet of the five β-strands, four parallel and one, β3, antiparallel. The 18-residue αB and the 5-residue αC lie below the sheet, while a combination of the 11-residue αA and four of the loops extend above the sheet on two sides to form a cleft that has the Zn^{2+} ion near its bottom. This cleft is 22–26 Å long and 10–11 Å deep with a wider end, 20 Å backbone-to-backbone, flanked by αA–loop A2 and loop 4B, and a narrower end, 8 Å, flanked by loops 34 and 5C.

The Zn^{2+} is firmly anchored to the protein by three side-chain ligands, His^{17}, His^{122}, and Cys^{130}, and connected to the hydroxyl group of Tyr^{46} through a water molecule (Fig. 1*D*). The Zn–ligand bond distances are 2.15 Å (Zn–S, Cys^{130}), 2.52 Å (Zn–N, His^{17}), 2.67 Å (Zn–N, His^{122}), and 2.83 Å (Zn–O, water molecule) and have nearly tetrahedral geometry. The distance between the hydroxyl group of Tyr^{46} and the water molecule is 3.02 Å. The Zn–ligand bond distances were not constrained during refinement. His^{122} and Cys^{130} are on one side of the cleft in loop 5C, His^{17} is in strand β1 at the bottom of the cleft, and Tyr^{46} is in loop A2 on the other side of the cleft from His^{122} and Cys^{130}.

In the AK6 crystal, the N-terminal amino group of one molecule extends toward the cleft of the neighboring molecule, contacting the side chains of Trp^{35} and Glu^{38} in αA. Apparently, the additional four amino acids at the N terminus of wild-type T7 lysozyme are not easily accommodated in the crystal structure, as reflected both in the difficulty of crystallizing the wild-type protein and in the disorder of the N-terminal residues.

Zinc Is Required for Amidase Activity but Not for Inhibition of Transcription. The position of Zn^{2+} at the bottom of the cleft and its coordination to a water molecule make it seem likely to be a cofactor for the amidase activity of T7 lysozyme. Coordination to three protein ligands and a water molecule is found universally in enzymes in which Zn^{2+} has a catalytic role, whereas coordination directly to four protein ligands is typical in proteins where Zn^{2+} atoms play a structural role (16).

Wild-type T7 lysozyme purified in the absence of added Zn^{2+} typically resolves into two or more peaks upon column chromatography, an observation that led to the discovery that T7 lysozyme contains zinc (J. Flanagan and K. MacKenzie, personal communication). The profile shown in Fig.

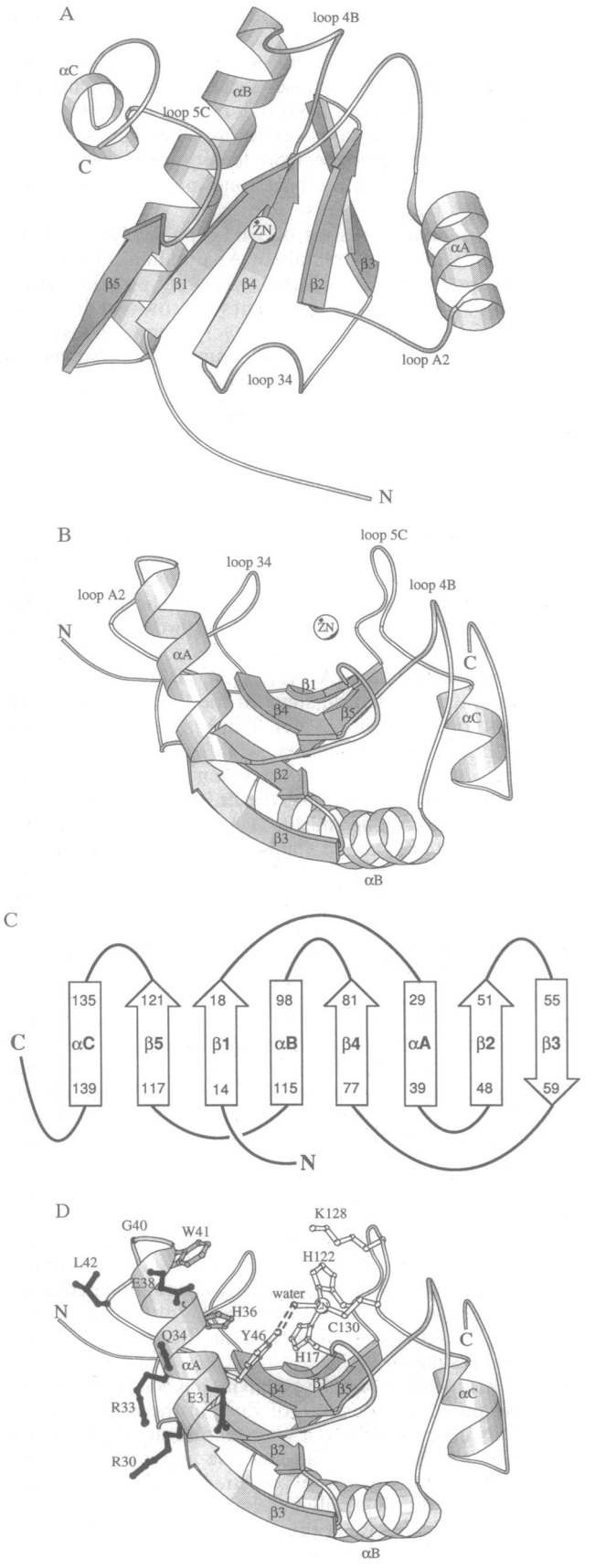

FIG. 1. Structure of T7 lysozyme mutant AK6. (*A*) Looking down on the cleft from above, which allows easy tracing of the chain. (*B*) Looking through the cleft from the wide end to the narrow end, approximately from upper right to lower left in *A*. The left side of the cleft is formed by αA–loop A2 and loop 34, the right side by loops 4B and 5C. The wide end of the cleft, at the front, is flanked by αA–loop A2 and loop 4B; the narrow end, at the back, is flanked by loops 34 and 5C. (*C*) Locations of structural elements in the amino acid sequence. (*D*) Same view as in *B*, showing side chains of certain amino acids implicated in amidase activity (unshaded) or inhibition of T7 RNA polymerase (darkly shaded). Trp[41] and His[36] are shown with intermediate shading because replacements of these residues have intermediate effects on both activities.

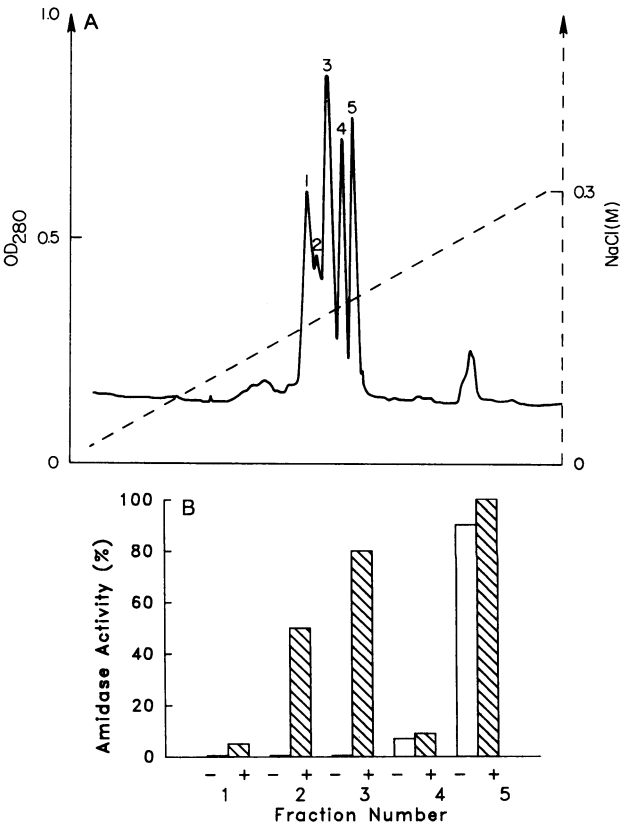

FIG. 2. Amidase activities of different fractions of T7 lysozyme purified in the absence of added Zn^{2+}. (*A*) Profile of wild-type T7 lysozyme chromatographed on a Mono S column. Peaks 1–5 were collected in separate fractions. (*B*) Amidase activity in the absence (−) or presence (+) of Zn^{2+}. Amidase activities are plotted relative to that of fraction 5 in the presence of Zn^{2+}. In this experiment, the specific activity of hen egg-white lysozyme was about 200 × 10^3 units/mg and that of the Zn^{2+}-containing fraction 5 was about 1800 × 10^3 units/mg, comparable to that observed for T7 lysozyme that had been purified in the presence of Zn^{2+}.

2*A* has five peaks, which were fractionated and assayed for activity. All five fractions had comparable ability to inhibit transcription by purified T7 RNA polymerase in the absence of added Zn^{2+}, and all bound T7 RNA polymerase equally well in a gel assay in the absence of any divalent ion. However, these fractions differed markedly in amidase activity, as measured in a lysozyme assay with EDTA-treated *E. coli* cells (Fig. 2*B*).

Fraction 5 had full amidase activity in the presence or absence of added Zn^{2+}, similar to T7 lysozyme purified in the presence of Zn^{2+}, and presumably contained fully active protein that had retained Zn^{2+} through the purification. Fraction 3 had undetectable amidase activity in the absence of Zn^{2+} but full activity in its presence. Apparently the protein in fraction 3 was inactive because it had lost Zn^{2+} but could recover full amidase activity when Zn^{2+} was added. Consistent with this interpretation, *o*-phenanthroline, a strong Zn^{2+} chelator, gradually inactivated the amidase activity of fraction 5, but activity was restored by adding Zn^{2+}.

Table 2. Properties of T7 lysozyme mutants

Mutation*	Structural element(s)	Suppressor mutation†	Polymerase inhibition‡	Amidase activity§
A1MD		Sup		
R2S		Sup		
V3G		Sup		
F5L		Sup		
F5S		Sup		
R8C		Sup		
R8H		Sup		
H17Q	β1, Zn		+	−
H17N			±	−
H17R			−	−
R30H	αA	Sup		
E31Q	αA		+++	+++
E31K			−	+++
R33S	αA	Sup		
R33L		Sup		
R33H		Sup		
Q34R	αA	Sup		
W35L	αA		+++	+++
W35H			+++	+++
W35S			+++	+++
W35C			++	+++
W35F			++	++
H36N	αA		++	+
H36C			++	+
H36Q			±	+
H36Y			++	−
H36R			−	−
E38G	αA	Sup		
Q39E	αA		+++	+++
Q39H			++	+++
Q39R			++	+++
G40R	A2	Sup		
G40V		Sup		
W41C	A2		+++	++
W41S			+++	+
W41L			++	+
W41R			+	−
L42F	A2		+++	++
L42I			+	++
L42P		Sup		
L42R		Sup		
Y46F	A2, Zn-H_2O		+++	−
Y46L			±	−
Y46D			−	−
G59E	β3	Sup		
S76Y	34	Sup		
G83D	4B	Sup		
L110P	αB	Sup		
A117D	β5	Sup		
K128N	5C		+++	±
K128T			+++	±
K128Q			+++	−
K128W			+++	−
K128Y			+++	−
K128M			+++	−
K128I			+++	−

Suppressor mutations are described in the text. The other mutations were generated by site-directed mutagenesis of a clone of T7 lysozyme in the pALTER-1 vector (Promega) under the control of a T7 promoter in the Altered Sites mutagenesis system (Promega) using oligonucleotides with a degenerate sequence at the target codon.

*Mutations are identified by the one-letter code for the wild-type amino acid followed by the residue number and then the one-letter code for the mutant amino acid. Mutations were identified and amino acid substitutions were inferred from DNA sequencing.

†Sup mutations should have reduced inhibition of T7 RNA polymerase.

Fractions 1 and 4 behaved similarly to fractions 3 and 5, except that their maximum amidase activity in the presence of Zn^{2+} was only about 10% that of fractions 3 and 5. Most of the activity of fraction 2 in the presence of Zn^{2+} was probably due to contamination with the protein of fraction 3. Some other factor must have limited the amidase activity of the proteins in fractions 1, 2, and 4, but not their ability to inhibit polymerase. We did not determine what other factor(s) might have been responsible.

We tested whether metal ions other than Zn^{2+} could activate the amidase of fraction 3. Addition of Mg^{2+} had no effect, Ca^{2+} had little if any effect, Mn^{2+} appeared to stimulate some activity, and Co^{2+} stimulated full activity.

Clearly, the naturally occurring Zn^{2+} is essential for the amidase activity of T7 lysozyme but not for its ability to inhibit T7 RNA polymerase. Thus, Zn^{2+} seems likely to have a catalytic function but unlikely to have an important structural role.

Amidase Catalytic Site. Being an amidase, T7 lysozyme might be expected to have a catalytic action similar to that of two well-characterized Zn^{2+} proteases, carboxypeptidase A (17) and thermolysin (18), which have similar active sites and similar catalytic mechanisms. Critical steps in the proposed general base mechanism for catalysis by these two enzymes include (*i*) interaction of a positively charged residue (Arg^{127} in carboxypeptidase A and His^{231} in thermolysin) with the substrate carbonyl; (*ii*) nucleophilic attack by a water molecule, promoted by the Zn^{2+} and a negatively charged residue (Glu^{270} in carboxypeptidase A and Glu^{143} in thermolysin); and (*iii*) resolution of the intermediate and donation of a hydrogen to the leaving amino group.

We identified potential catalytic residues within the cleft by superimposing the Zn^{2+} and the three protein ligands of T7 lysozyme with those of carboxypeptidase A and thermolysin. The bond angles between Zn^{2+} ligands could be aligned closely in only one orientation, where His^{122}, Cys^{130}, and His^{17} in T7 lysozyme correspond to His^{69}, Glu^{72}, and His^{196} in carboxypeptidase A and to Glu^{166}, His^{146}, and His^{142} in thermolysin. In this superposition, Lys^{128} of T7 lysozyme is in the position of the positively charged residue in the two proteases and Tyr^{46} is in the position of the negatively charged residue, suggesting that these two residues may have a critical role in catalysis.

Results of site-directed mutagenesis support the idea that Lys^{128} and Tyr^{46} are important for amidase activity (Table 2). All seven substitutions obtained for Lys^{128} abolished or greatly reduced amidase activity while retaining full inhibition of T7 RNA polymerase. Both of the two substitutions that retained slight residual activity, Asn and Thr, would have the potential to form a hydrogen bond with the carbonyl oxygen of the substrate amide, consistent with Lys^{128} functioning by interacting with this group. Replacing Tyr^{46} with Phe also abolished amidase activity without affecting the ability to inhibit transcription, consistent with a role for the tyrosine hydroxyl group in activating the water molecule. Replacing Tyr^{46} with Leu or Asp rather than Phe abolished both amidase and inhibitory activity, suggesting that the aromatic ring of Tyr^{46} may have a significant structural role as well.

Substitutions were also made for His^{17}, one of the three Zn^{2+} ligands (Table 2). As expected, all three substitutions

‡Inhibition of T7 RNA polymerase was estimated from the plaque size of wild-type T7 plated on *E. coli* HMS174 containing the mutant plasmid (1): normal plaques indicated no inhibition (−) and tiny plaques full inhibition (+++).

§Amidase activity was estimated by ability of chloroform to lyse a mid-logarithmic tryptone broth culture of *E. coli* HMS174 containing the mutant plasmid: +++, clearing in 1–2 min; ++, clearing in 3–5 min; +, viscous in 1–2 min and partial clearing in 3–5 min; ±, viscous in 3–5 min but only slight clearing by 5 min; −, no sign of lysis after 3 hr.

eliminated amidase activity. However, these mutants also lost at least some ability to inhibit T7 RNA polymerase, suggesting that these substitutions also affected the structure more generally.

Comparison with Other Lysozymes. T7 lysozyme has a lytic activity similar to that of egg-white or T4 lysozyme, but it cuts a different bond in the peptidoglycan layer (7) and, even though all three proteins have a cleft (19), is structurally very different from them. The critical residues for catalysis by egg-white and T4 lysozyme are glutamic and aspartic residues located on opposite sides of the cleft, but no acidic residues are found inside the cleft of T7 lysozyme. In contrast to the other lysozymes, T7 lysozyme had no apparent activity against the Gram-positive bacterium *Micrococcus lysodeikticus*, a usual substrate in lysozyme assays. This observation may offer an approach to learning more about the substrate specificity of T7 lysozyme and may also have evolutionary significance, since T7-like phages have been found to infect a range of Gram-negative bacteria (20) but have not been reported for Gram-positive bacteria.

Interaction with T7 RNA Polymerase. In contrast to multifunctional proteins that contain multiple domains, the bifunctional T7 lysozyme is a single-domain globular protein. The cleft is clearly the site of amidase activity. What is the site of interaction with T7 RNA polymerase?

We have done considerable mutational analysis of the interaction between T7 RNA polymerase and T7 lysozyme (X.Z. and F.W.S., unpublished data). Several mutations in T7 RNA polymerase prevent phage growth because the mutant polymerase is hypersensitive to inhibition by T7 lysozyme. Suppressor mutations that allow such phages to grow were all in T7 lysozyme. These mutant lysozymes should be deficient in the ability to interact with T7 RNA polymerase but retain enough amidase activity to form a plaque, and deficiency in binding or inhibition of T7 RNA polymerase was confirmed directly for several of them. The site of each suppressor mutation was determined by DNA sequencing of 30 such mutants, which affected 16 different amino acids in T7 lysozyme (Table 2).

The N terminus of T7 lysozyme appears to be important in interacting with T7 RNA polymerase, since suppressor mutations were found in five of the first eight amino acids. (The AK6 mutant, lacking residues 2–5, was constructed because of these results.) A second cluster of suppressors affected six amino acids between residues 30 and 42 on the outer side of helix αA and near the beginning of the A2 loop (Fig. 1*D*). A surface involving this region and the N terminus (which in wild-type lysozyme would contain four more residues) seems likely to be the site of interaction with T7 RNA polymerase. Suppressors at residues 59 (the end of β3), 76 (just ahead of β4), and 117 (at the beginning of β5) are in the same general area. However, they and the two suppressors at residues 83 (past the end of β4) and 110 (near the end of αB) are buried in the structure and seem more likely to exert their effect on the structure as a whole.

Helix αA seems to be part of the surface that interacts with T7 RNA polymerase, but it also forms a part of one wall of the cleft and could, therefore, be involved in binding the amidase substrate. To investigate this further, we mutated additional residues of αA (Table 2). Replacement of Glu^{31} by Lys eliminated the ability to inhibit polymerase without affecting amidase activity, but replacement by Gln had no effect. Five different replacements of Trp^{35} and four replacements of Gln^{39}, both on the inner side of the cleft, had little effect on either activity. On the other hand, replacement of His^{36}, also on the inner side of the cleft, and Trp^{41}, in the beginning of loop A2, had variable effects, usually affecting amidase activity more than polymerase inhibition. The outer surface of helix αA certainly seems to be involved in interaction with T7 RNA polymerase, but it is not clear to what extent the inner surface may interact with the amidase substrate.

The 883-amino acid T7 RNA polymerase is much larger than the 150-amino acid T7 lysozyme, and its binding to one side of the cleft might be expected to block the entry of the amidase substrate or to interfere more directly with the catalytic process. Indeed, we found that a slight molar excess of polymerase over lysozyme strongly inhibited the amidase activity of wild-type but not AK6 lysozyme. Perhaps this inhibition has a role in controlling lysis during T7 infection.

Physiological Role. T7 lysozyme combines two seemingly unrelated functions in one small protein. These functions are not separated into independent domains, and an individual molecule seems able to perform only one function at a time. This mutual exclusion may be important for the sequential functioning of T7 lysozyme during T7 infection, where in the middle stages it provides a feedback mechanism for controlling transcription and in the late stages it participates in lysis. The interaction between T7 lysozyme and T7 RNA polymerase is also related somehow to replication (1, 2), and replication is related to lysis (2, 21). T7 lysozyme appears to be a link among these processes, and knowledge of its structure, together with the recently determined structure of T7 RNA polymerase (22), should aid in elucidation of their interconnections.

Work at Brookhaven National Laboratory was supported by National Institutes of Health Grant GM21872 and by the Office of Health and Environmental Research of the U.S. Department of Energy.

1. Moffatt, B. A. & Studier, F. W. (1987) *Cell* **49**, 221–227.
2. Studier, F. W. (1972) *Science* **176**, 367–376.
3. Silberstein, S., Inouye, M. & Studier, F. W. (1975) *J. Mol. Biol.* **96**, 1–11.
4. McAllister, W. T. & Wu, H.-L. (1978) *Proc. Natl. Acad. Sci. USA* **75**, 804–808.
5. Studier, F. W. (1991) *J. Mol. Biol.* **219**, 37–44.
6. Studier, F. W., Rosenberg, A. H., Dunn, J. J. & Dubendorff, J. W. (1990) *Methods Enzymol.* **185**, 60–89.
7. Inouye, M., Arnheim, N. & Sternglanz, R. (1973) *J. Biol. Chem.* **248**, 7247–7252.
8. Dunn, J. J. & Studier, F. W. (1983) *J. Mol. Biol.* **166**, 477–535.
9. Messerschmidt, A. & Pflugrath, J. W. (1987) *J. Appl. Crystallogr.* **20**, 306–315.
10. Kabsch, W. (1988) *J. Appl. Crystallogr.* **21**, 916–924.
11. Weissman, L. (1982) in *Computational Crystallography*, ed. Sayre, D. (Oxford Univ. Press, Oxford), pp. 56–63.
12. Steigemann, W. (1974) Ph.D. Thesis (Technische Universität, Munich).
13. Jones, T. A. (1978) *J. Appl. Crystallogr.* **11**, 268–272.
14. Brunger, A. T., Kuriyan, J. & Karplus, M. (1987) *Science* **235**, 458–460.
15. Schleif, R., Greenblatt, J. & Davis, R. W. (1971) *J. Mol. Biol.* **59**, 127–150.
16. Vallee, B. L. & Auld, D. S. (1990) *Proc. Natl. Acad. Sci. USA* **87**, 220–224.
17. Christianson, D. W. & Lipscomb, W. N. (1989) *Acc. Chem. Res.* **22**, 62–69.
18. Matthews, B. W. (1988) *Acc. Chem. Res.* **21**, 333–340.
19. Matthews, B. W., Remington, S. J., Grutter, M. G. & Anderson, W. F. (1981) *J. Mol. Biol.* **147**, 545–558.
20. Hausmann, R. (1988) in *The Bacteriophages*, ed. Calendar, R. (Plenum, New York), Vol. 1, pp. 259–289.
21. Studier, F. W. (1969) *Virology* **39**, 562–574.
22. Sousa, R., Chung, Y. J., Rose, J. P. & Wang, B.-C. (1993) *Nature (London)* **364**, 593–599.